Fabrication of Self-Biased Circulators with Integrated Hexagonal Microwave Ferrites Using LTCC Technology

M. Heidenreich, J. Schur, J. Müller, B. Capraro, W. Gitzel, A. F. Jacob, J. Töpfer

Next-generation magnetic microwave devices for satellite communication technologies require passive components including circulators that manipulate electromagnetic signals at high frequency. For this, circulators have to be integrated into LTCC microwave communication modules. Substituted M-type hexagonal ferrites represent a class of microwave magnetic materials with self-biasing ability and ferromagnetic resonance frequencies in the range of 25–50 GHz. The authors report on different options for integration of self-biased ferrites into LTCC multilayer devices, including drop-in sintered ferrites, and cofiring of screen-printed ferrite layers or ferrite tapes. Sintered substituted hexagonal microwave ferrites with preferential orientation were fabricated by compaction of powders in a magnetic field and sintering, whereas ferrite thick films were prepared by screen-printing, drying in an external magnetic field, and sintering at 900 °C. The magnetic texture of the ferrites is characterised using XRD, EBSD, and magnetic measurements. The substituted ferrites exhibit a ferromagnetic resonance frequency at about 30 GHz with nonreciprocal properties, and were integrated in a LTCC Y-junction circulator. Test results indicate that hexagonal ferrites are promising materials for self-biased circulators fabricated in LTCC technology for microwave components at K_a-band frequencies around 30 GHz.

Manuel Heidenreich, Jörg Töpfer
Department of SciTec
Ernst Abbe Hochschule Jena
07745 Jena, Germany

Johannes Schur, Jens Müller
Technical University Ilmenau
98693 Ilmenau, Germany

Beate Capraro
Fraunhofer IKTS
07629 Hermsdorf, Germany

Wanja Gitzel, Arne F. Jacob
Institute of High-Frequency Technology
Hamburg University of Technology
21073 Hamburg, Germany

Corresponding author: J. Töpfer
E-mail: joerg.toepfer@eah-jena.de

Keywords: hexagonal ferrites, texture, magnetic properties, microwave properties

1 Introduction

Recent satellite communication systems rely on geostationary earth orbit satellites with large footprint and large number of spot beams. Alternatively, more complex low earth orbit systems with larger numbers of miniature satellites and with lower required transmitting power have been developed [1]. New satellite generations require higher data rates (Very High Throughput Satellites VHTS) and larger bandwidths which may be realised using higher operating frequencies. Moreover, miniaturisation and reduction of components and integration costs are important requirements. Because of its enormous miniaturisation potential and its proven reliability in space, the Low Temperature Cofired Ceramics (LTCC) technology exhibits high potential for the fabrication of miniaturised satellite communication modules [2].

The KERAMIS network in Germany has developed and verified LTCC-based RF equipment for satellite communications in the K_a-band, including reconfigurable switch matrix, amplifiers, and 30–20 GHz down-converter units [3]. Circulators are also important passive microwave components and are used as duplexers or isolators. They allow to send and receive microwave signals simultaneously through a single antenna. Y-junction circulators allow to pass signals from port 1 to port 3 with a connected antenna, while isolating port 2.

Likewise, signals entering port 3 will be allowed to pass through port 2, while isolating port 1. These devices typically rely on soft ferrites in combination with an external bias magnet to generate non-reciprocal behaviour and to adjust the Ferromagnetic Resonance Frequency (FMR) near the circulator's operating frequency. The necessity of bulky bias magnets contradicts the need for miniaturisation, especially for high frequency bands, e.g., K- and K_a-bands. For such high operating frequency, self-biased circulators based on hexagonal ferrites are used which allow for realising compact systems.

Polycrystalline $(Ba/Sr)Fe_{12}O_{19}$ ferrites with hexagonal M-type crystal structure are

well known for applications as permanent magnets. The crystal structure of M-type ferrite (space group $P6_3/mmc$) is formed by a stacking sequence of R- and S-blocks as SRS*R*, where * denotes a 180° rotation around the c-axis. The unit cell contains two formulae $BaFe_{12}O_{19}$ (z = 2). The ferric ions occupy 12k sites (octahedral sites between R- and S-blocks), tetrahedral $4f_1$) sites (in S-blocks), octahedral $4f_2$) sites (in R-blocks), bipyramidal 2b sites (in R-blocks) and octahedral 2a sites in S-blocks.

The magnetic moments of the Fe ions in the 12k, 2b and 2a sites are parallel to the c-axis. The magnetic moments of the $4f_1$ and $4f_2$ sites are antiparallel to the c-axis [4, 5]. In addition, their high-frequency magnetic properties qualify them as promising non-reciprocal microwave materials [6–9]. Due to their significant magneto-crystalline anisotropy and remanence, hexagonal ferrites are self-biasing and thus no additional bias magnets are needed for circulator applications [8].

Barium ferrite, $BaFe_{12}O_{19}$, exhibits a magneto-crystalline anisotropy of $K_1 = 10^6$ erg/cm³ which, according to $H_a = 2K_1/M_s$, results in an anisotropy field H_a of 17 kOe [5]. A ferromagnetic resonance was measured on single crystals at $f_R = 46$ GHz [10]. Substitution of Fe^{3+} ions with diamagnetic cations allows effective tailoring of the magnetic and microwave properties of M-type ferrites: substitution of Al^{3+} and Ga^{3+} increases H_a, whereas Sc^{3+}-, In^{3+}-, and Zn^{2+}/Sn^{4+}-substitution reduces the anisotropy field H_a and the ferromagnetic resonance frequency (FMR) [11–15]. The synthesis, sintering behaviour, and magnetic properties of substituted $BaMe_xFe_{12-x}O_{19}$ ferrites with Me = Sc and In ($0 \leq x \leq 2$) as well as their microwave resonance properties were studied recently [13, 14]. Sc-substituted ferrites with x = 0,5 exhibit a saturation magnetisation at room temperature of $M_s = 64$ emu/g, a coercivity of 0,36 kOe, and a FMR at 30 GHz [14]. Such substituted ferrites are appropriate for the fabrication of self-biased circulators [16].

The integration of microwave ferrites into LTCC multilayer microwave modules for satellite communications is a novel and challenging topic. The standard approach is to drop a pre-sintered ferrite puck or disk into a cavity in the LTCC substrate [17]. Alternatively, circulators are integrated as Surface-Mount Device (SMD). Printing of ferrites on alumina substrates and subsequent hot-press sintering at high temperatures has already been proposed [18]. Recently, the integration of screen-printed anisotropic ferrite thick films has been demonstrated [19].

Here, the authors report on the fabrication and microwave properties of LTCC-based circulators using self-biased substituted hexagonal ferrites as magnetic components. Different technology options were tested:

- drop-in of sintered textured ferrite pellets,
- integration of screen-printed oriented ferrite films, and
- integration of ferrite tapes.

The authors address the synthesis and magnetic properties of the ferrites and ferrite films, details of LTCC integration technologies, as well resulting circulator characteristics. Such LTCC integrated circulators exhibit great potential as microwave components embedded in ceramic multilayer modules operating at K_a-band frequencies.

2 Experimental

$BaMe_xFe_{12-x}O_{19}$ and $SrFe_{12}O_{19}$ powders (Me–Sc, In, $Zn_{0,5}/Sn_{0,5}$) were prepared by weighing Fe_2O_3, Ba- or $SrCO_3$, Sc_2O_3, In_2O_3, ZnO and SnO_2, and wet mixing for 12 h with zirconia grinding balls in water. The powder mixture was calcined for 4 h at 1300 °C. Next, the calcined powders were wet milled with zirconia grinding media in a planetary ball mill for 9 h.

After addition of PVA pressing aid and compaction, the pellets were sintered at 1400 °C for 4 h. For the fabrication of ferrites with magnetic orientation, a water-based slurry of the calcined ferrite particles was wet-pressed in a magnetic field. After drying, the anisotropic samples were sintered at 1400 °C. For low-temperature sintering, a mixture of 3 mass-% of Bi–B–Si–Zn glass (BBSZ) and 2 mass-% CuO powder was added as sintering aid during milling. A ferrite paste was prepared by mixing the ferrite powder with terpineol and cellulose binders with a solid content of 62,5 mass-%. The paste was screen-printed on CT708 LTCC tapes and dried at 150 °C for 2 h. During drying, a static magnetic field generated by two SmCo permanent magnets (H = 6 kOe) was applied perpendicular to or within the film direction. The films were positioned in the airgap between the magnets, and the magnet assembly was placed in a drying oven. Next, the films were heated to 500 °C with 0,5 K/min for binder burnout, then with 4 K/min to 900 °C, and sintered at 900 °C for 4 h. A ferrite tape was fabricated using a slurry of the ferrite powder with MEK/ethanol solvent, dispersant and binder and a doctor blade casting machine. For cofiring experiments, two ferrite tape layers were stacked between two CT708 LTCC layers on top and bottom and laminated. The CT708/ferrite laminates were heated with 2 K/min to 900 °C and sintered for 2 h.

The particle size of the ferrite powder was measured using laser diffraction (Malvern Mastersizer 2000). The specific surface of the powder was measured by BET nitrogen adsorption (Nova 2000, Quantachrome Instruments). The bulk density of sintered samples was determined using Archimedes' method. Shrinkage measurements were made on cylindrical compacts using a Netzsch DIL402 dilatometer with 4 K/min heating rate. The microstructure of the sintered ferrites was investigated using an Ultra 55 Field Emission Scanning Electron Microscope (Zeiss) equipped with a EBSD camera. X-ray patterns were recorded with a Bruker AXS D8 Advance diffractometer using Co K_α radiation. Lattice parameters were obtained through Rietveld refinements using Bruker Topas 6 software. The microstructural anisotropy was characterised by measuring pole figures (Bruker D8 Discover diffractometer) of the (006), (107) and (114) lattice planes with a tilt angle Psi $\chi = 0–78°$ (increment $\Delta\chi = 3°$) in a full circle Phi $\phi = 0–360°$ (increment $\Delta\phi$ = various). Pole figures were calculated using Bruker Texture 4.1; further data evaluation and plotting was performed using the MTEX toolbox 5.1.1 [20] for MATLAB (The MathWorks Inc., Natick, USA). Hysteresis loops of the ferrite powders and films were measured at room temperature using a VSM magnetometer (MicroMag TM 3900, Princeton Measurements Corp./US).

The ferromagnetic resonant frequency was determined by return loss measurements in short-circuited waveguides. The sintered ferrites were cut into thin rectangular bars which were placed in front of the short circuit. The measurements were performed with an Agilent PNA E8361A network analyzer in three frequency bands using WR-42

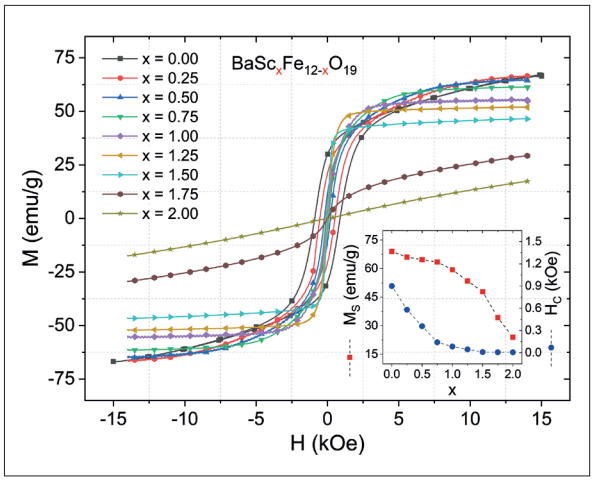

Fig. 1 Room-temperature hysteresis loops of $BaFe_{12-x}Sc_xO_{19}$ and saturation magnetisation and coercivity vs. Sc-substitution x (inset)

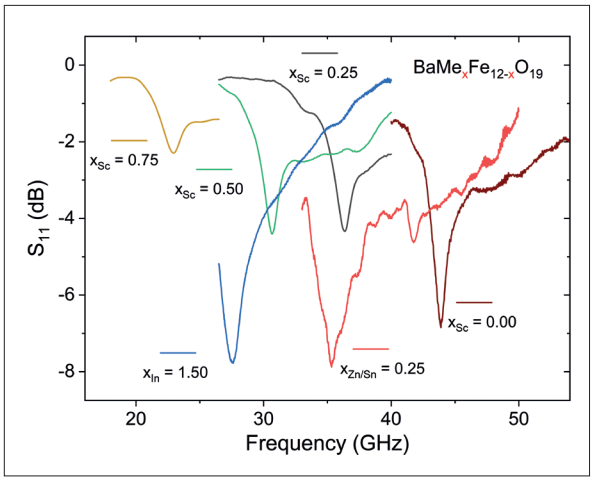

Fig. 2 Reflection coefficient vs. frequency for substituted ferrites $BaFe_{12-x}Me_xO_{19}$ with Me = Sc, In, and Zn/Sn

(18–26,5 GHz), WR-28 (26,5–40 GHz), and WR-19 (40–60 GHz) rectangular waveguides. No external magnetic field was applied during the measurements. The fabricated microstrip Y-junction circulators featured transitions to coplanar waveguides and were also measured using coplanar probes. The circulator measurements were carried out with a Rohde & Schwarz ZVA50 4-Port vector network analyser in the range from 10–50 GHz.

3 Results and discussion

3.1 Microwave hexagonal ferrite properties

The calcined $BaMe_xFe_{12-x}O_{19}$ ferrite powders consist of a single M-type ferrite phase according to X-ray diffraction (not shown here). After milling, the mean particle size of the powder is d_{50} = 3 µm as measured with laser diffraction and exhibits a specific surface of 10 m²/g. After sintering the samples at 1400 °C densities of 95–96 % were achieved. The static magnetic properties of the substituted ferrites $BaMe_xFe_{12-x}O_{19}$ vary with the substitution rate x.

As an example, the hysteresis loops at room temperature for Me = Sc are shown in Fig. 1. BaM ferrite (x = 0) with uniaxial anisotropy exhibits a broad M-H loop. With increasing Sc-content x, the character of the hysteresis loop changes from hard into semi-hard and soft magnetic at x >1. The corresponding variation of M_s and H_c of the Sc-substituted ferrites vs. x is shown in the inset of Fig. 1. The saturation magnetisation M_s is reduced from 69 emu/g at x = 0–59 emu/g at x = 1,0, or 48 emu/g, respectively, at x = 1,5. Simultaneously, the coercivity drops from H_c = 0,9 kOe for x = 0 to H_c = 84 Oe for x = 1,0. The reduction of M_s is caused by the substitution of Fe^{3+} ions with a magnetic moment of 5 µB by nonmagnetic Sc^{3+} ions. Based on the Gorter ferrimagnetic model of co-linear spin arrangements, Ba ferrite has a saturation magnetisation of 20 µB (100,5 emu/g) at 4 K and of about 70 emu/g at 298 K [4, 5]. It has been demonstrated by Mössbauer spectroscopy [21], that Sc^{3+} cations prefer to occupy R-block octahedral $4f_2$ and 2b sites. Since $4f_2$ sites contribute to the spin-down magnetic sublattice, the replacement of ferric by nonmagnetic ions would increase the total magnetic moment.

Therefore, an assumed antiparallel spin arrangement is not able to explain the reduction of M_s. Moreover, weakening of the super-exchange interactions results in different magnetic configurations with lower net magnetic moments, composed of helical blocks with different angles between adjacent blocks [22].

The decrease of coercivity with x (Fig. 1) is attributed to a reduction of the uniaxial magneto-crystalline anisotropy. As already demonstrated by Röschmann et al. [12], the anisotropy field in $BaSc_xFe_{12-x}O_{19}$ decreases from 17 kOe for x = 0 to about 7 kOe for x = 1, up to the disappearance of the uniaxial anisotropy at about x = 1,7.

The microwave properties of substituted hexagonal M-type ferrites $BaMe_xFe_{12-x}O_{19}$ were measured using a waveguide arrangement and the observed reflection coefficient S_{11} exhibits ferromagnetic resonance phenomena (Fig. 2). The ferromagnetic resonance frequency decreases with increasing Sc-concentration, which is consistent with the reduced coercivity H_c and anisotropy field H_a for increasing x. The magnitude of the measured reflection coefficient at resonance is affected by the internal magnetic field of the ferrite, which is not only determined by the ferrite anisotropy field, but also by demagnetising fields (which are a function of size and shape). Ba-ferrite has its FMR at about f_r = 44 GHz, which agrees with results by Ustinov et al. [23], who report a resonance frequency of single-crystalline Ba ferrite films at zero applied field of f_r = 47 GHz. For $BaSc_xFe_{12-x}O_{19}$, the FMR is observed at f_r = 30 GHz for x = 0,5; at x ≥ 0,75 the resonances are below 20 GHz (Fig. 2). The decrease of f_r with x in the case of $BaIn_xFe_{12-x}O_{19}$ is less pronounced [14] and for x = 1,5 the FMR appears at about f_r = 28 GHz (Fig. 2).

In the series $BaZn_xSn_xFe_{12-2x}O_{19}$, the FMR for x = 0,25 is at about 35 GHz (Fig. 2). For the experiments reported in the following sections, a Sc-substituted ferrite with x = 0,5 was used.

3.1.1 Drop-in sintered ferrite integration

The integration of sintered ferrite samples into cavities of LTCC multilayer structures is a well-known option for the fabrication of circulators. In order to achieve self-biasing

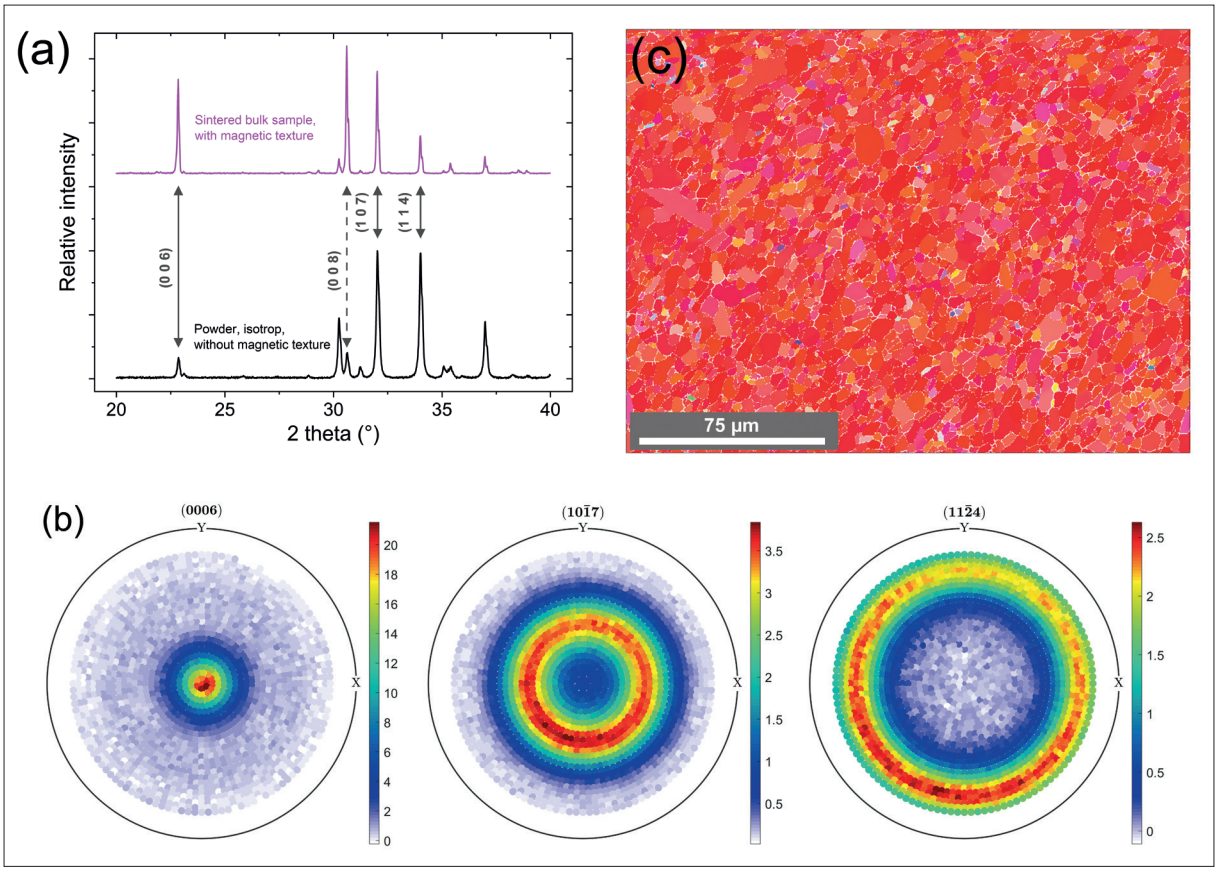

Fig. 3 a–c X-ray diffraction patterns of $BaSc_{0,5}Fe_{11,5}O_{19}$ ferrite isotropic powder (bottom) and ferrite textured with magnetic field and sintered (top) **(a)**; XRD pole figures of (006), (107) and (114) reflexes of textured and sintered ferrites **(b)**; EBSD map of a textured and sintered ferrite **(c)**

operation of the used microwave ferrite, a sufficient uniaxial magneto-crystalline anisotropy of the ferrite is required. This allows for the formation of a preferential crystallographic and magnetic orientation of the ferrite particles through pressing a slurry of the ferrite particles in a magnetic field and subsequent sintering. The extent of crystallographic orientation (texture) was characterised using X-Ray Diffraction (XRD). A diffraction pattern of a calcined isotropic ferrite powder is contrasted with that of a sintered bulk sample with crystallographic and magnetic texture (Fig. 3 a). Whereas the powder sample shows a typical distribution of peak intensities consistent with the frequency of appearance of individual lattice planes, the textured sample exhibits high intensities of (00l) lattice planes. Besides the (006) and (008) reflexes, also the (107) peak appears with high intensity. The Lotgering factor [24]

$$LF = \frac{P_{(00l)} - P_0}{1 - P_0} \qquad \text{(eq. 1)}$$

is used to estimate the extend of orientation in a textured sample with

$$P_{(00l)} = \frac{\sum I_{(00l)}}{\sum I_{(hkl)}} \quad P_0 = \frac{\sum I_{0(00l)}}{\sum I_{0(hkl)}} \qquad \text{(eq. 2)}$$

and $\sum I_{(00l)}$ as summation of peak intensities of all (00l) peaks and $\sum I_{(hkl)}$ as summation of all peak intensities of the textured sample. P_0 represents the summation of peak intensities of an isotropic, i.e. randomly oriented powder sample. The Lotgering factors of an isotropic and of a completely textured sample are zero and one, respectively. For the sintered textured Sc-substituted ferrite a LF of 0,69 was obtained, indicating a substantial, but not perfect degree of preferential orientation. LFs of non-substituted hexagonal ferrites used as permanent magnets exhibit a higher degree of texture with LFs of typically 0,8. This seems to be due to the larger magneto-crystalline anisotropy of the unsubstituted as compared to the Sc-substituted ferrite.

The authors have also characterised the texture of the sintered ferrites using XRD pole figure measurements with a Eulerian cradle. As example, pole figures of (006), (107) and (114) reflections (or (0006), (10$\bar{1}$7) and (11$\bar{2}$4) peaks in hexagonal indexing) were determined for sintered oriented ferrites (Fig. 3 b). Examination of the (006) pole figure reveals a strong texture. Similarly, the (107) and (114) pole figures with their observed rings are also indicative of a fibre texture.

These findings represent massive support for a strong preferential orientation of ferrite particles in the sintered sample. In addition, electron back scatter diffraction (EBSD) was used to map the grain orientation on a polished surface of a textured sintered ferrite (Fig. 3 c); grains with a (00l) orientation are shown in red. The EBSD map confirms a substantial c-axis preferential orientation of most grains. However, a significant number of grains shows different orientations in agreement with the results of the LF and XRD pole figure analysis. The EBSD map reveals a microstructure characterised by large grains up to several tens of

microns, which indicates significant grain growth during sintering at 1400 °C. Further optimization of the texture formation during wet pressing and of the microstructure formation during sintering is required.

It has been suggested, that bulk hexagonal ferrites are promising materials for circulators operating at high frequency, or even at K_a-band [25]. Recently, a self-biased circulator using bulk La/Co-substituted Sr ferrite was reported [26]. The drop-in integration of a sintered hexagonal ferrite into a cavity of LTCC multilayer tape stack is shown in Fig. 4. DuPont 951 was used as LTCC tape material. The exploded view of the LTCC multilayer circulator (Fig. 4 a) depicts the important components of the circulator, and Fig. 4 b describes the LTCC processing route. Separated by multiple LTCC tape layers, a ground plane and a resonator structure are screen-printed using Au paste onto individual LTCC tape layers. In the middle section, several LTCC green tapes with laser-cut cavities are stacked.

Next, the sintered ferrite sample with precise geometry, i.e., with height of 300 µm prepared by polishing, and lateral dimensions of about 1 mm diameter obtained by laser cutting, is dropped into the cavity. Finally, the upper LTCC tape layers including the printed resonator structure are stacked on top, and the whole multilayer stack is uniaxially laminated and cofired at 875 °C for 30 min. Initially, defects including warping, or formation of air gaps between the LTCC layers and the ferrite surface were observed as result of cofiring. It has been concluded, that a precise control of the thickness of the LTCC green tape stack as well of the ferrite height are crucial for obtaining error-free cofired samples. It was found, that even small deviations from the perfect cylindrical geometry of the ferrite pellet (small deviation from 90° angle and, consequently, different upper and lower diameters of the ferrite pellet) have to be taken into account, and proper dimensional design of the green LTCC tape layers for top- and bottom layers, as well as for cavity layers is required.

A small airgap between LTCC and ferrite after cofiring cannot be avoided due to thermal expansion mismatch. In order to optimise the positioning of the ferrite pellet in the cavity of the green LTCC stack in the centre position below the printed resonator, a carbon-tape ring (with exact geometry fabricated by laser machining) was placed in the cavity of the green tape stack. With the use of such sacrificial tape rings, the optimum ferrite placement was achieved. The carbon tape was removed during binder burnout of the multilayer stack before reaching the peak sintering temperature. To further reduce the dimensions of lateral and vertical airgaps between ferrite and LTCC, de-aeration channels were included into the LTCC stack to remove air from the cavities during shrinkage while sintering. The de-aeration channels were fabricated using carbon-tape as well. A common carbon-tape ring and de-aeration channel structure was fabricated by laser machining and integrated in the green multilayer stack. Finally, circulators with integrated sintered drop-in ferrites without airgaps (Fig. 4 c) and perfect position of the ferrite below the resonator were obtained after cofiring at 875 °C. A CT micrograph of a circulator with printed circulator structure, sintered cylindrical ferrite and de-aeration channels is shown in Fig. 4 d.

The geometry of the fabricated Y-junction circulator shown in Fig. 4 is characterised by many parameters, including the radius of the circular center conductor r_1 (500–750 µm), the width of the microstrip line w = 300 µm, the thickness of the Au thick film (10 µm), the ferrite thickness t_f of 300 µm, and the substrate thickness as the sum of the sintered LTCC layers thickness (about 500 µm). Optimizations of the geometry parameters in combination with simulations have been performed for different operational conditions (below or above FMR), and more details will be reported somewhere else [27].

To characterise the circulator performance, measurements of the S-parameters (S_{11}, S_{21} and S_{12}) as function of frequency were performed. The non-reciprocity NR is obtained from the difference (in dB) between S_{21} and S_{12} signals. As an example, the results of a drop-in circulator with r_1 = 700 µm and an unsubstituted Sr-ferrite are presented in Fig. 5. The FMR of that ferrite is at 45 GHz and the circulator yields an input reflection below –19 dB and an inser-

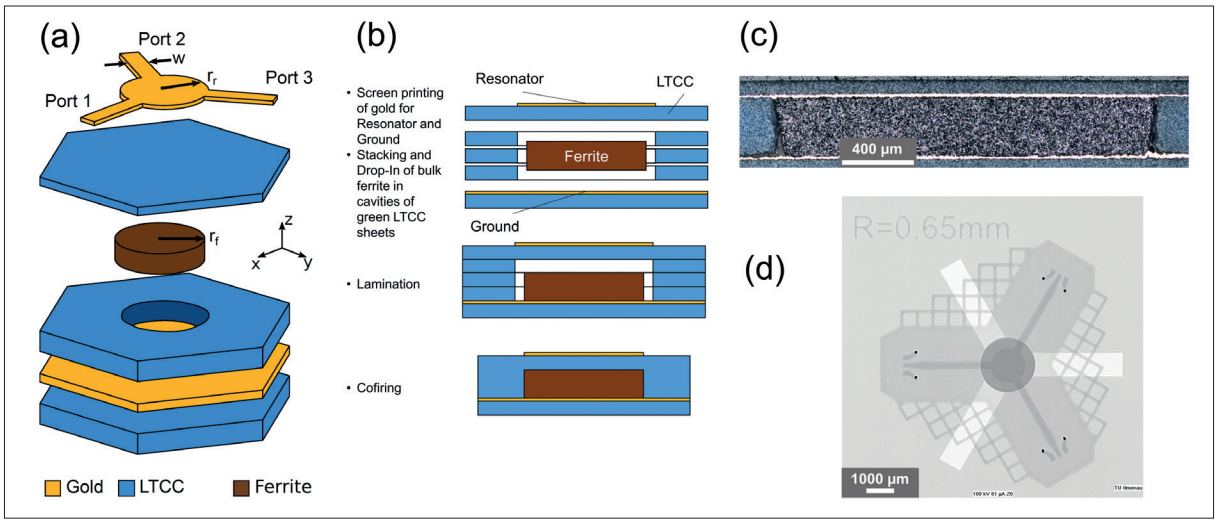

Fig. 4 a–d Drop-in sintered ferrite integration: exploded view of LTCC multilayer circulator **(a)**; scheme of LTCC fabrication technology route **(b)**; micrograph of cross-section of cofired circulator with integrated ferrite **(c)**; CT top view onto LTCC multilayer circulator with printed Au structure, drop-in ferrite; de-aeration channels **(d)**

tion loss of –6 dB in the frequency band below FMR. The measured nonreciprocity exceeds 15 dB in a 3 GHz band centred around at 40,8 GHz compared to 3,85 GHz and 40,6 GHz, respectively, in simulations. For simulation of the circulator, the material parameters used are $\varepsilon_r = 6{,}4$ and tan $\delta = 0{,}006$ for the LTCC substrate, a saturation magnetisation of 420 mT, a line width of 900 Oe, an internal magnetic field of 15 000 Oe, and a permittivity $\varepsilon_r = 15$ and loss factor of tan $\delta = 0{,}001$ for the ferrite.

3.1.2 LTCC integration of printed ferrite films

Without sintering additive, the Sc-substituted hexagonal ferrites are sintered at high temperatures. Dilatometric measurements (not shown here) indicated the maximum shrinkage rate to appear at $T_{MSR} = 1300$ °C and, consequently, the ferrites were sintered at 1370–1400 °C for compete densification [14]. To reduce the sintering temperature and enable low-temperature firing of ferrite printed films or tapes, a mixture of 3 mass-% BBSZ glass powder and 2 mass-% CuO was added as liquid phase sintering aid [19]. The sintering additives shift the temperature of maximum shrinkage rate down to at $T_{MSR} = 760$ °C (Fig. 6) and sintering of bulk samples with this additive mix at 900 °C gives densities of about 90 %. For cofiring of printed ferrite films or ferrite tapes with LTCC green tapes, the LTCC material system CT708 was used. Both materials, the low-firing hexagonal ferrite (with sintering additives) and CT708 show similar shrinkage behaviour (Fig. 6). In addition, the coefficients of thermal expansion (CTE) of the ferrite and of CT708 (10,8 ppm/K and 10,6 ppm/K (140–740 °C), respectively, are similar. Such little thermal expansion mismatch and similar shrinkage behaviour are prerequisites for successful cofiring of both materials at 900 °C [28].

Printing of ferrite paste onto CT708 tape and cofiring gives ferrite films with a thickness of about 12 µm for a single print. Thicker films up to 50 µm were fabricated by multiple printing cycles with intermediate drying. The printed ferrite films were dried in a magnetic field before cofiring to align the ferrite particles and generate a crystallographic and magnetic texture in the ferrite film. The sintered ferrite films

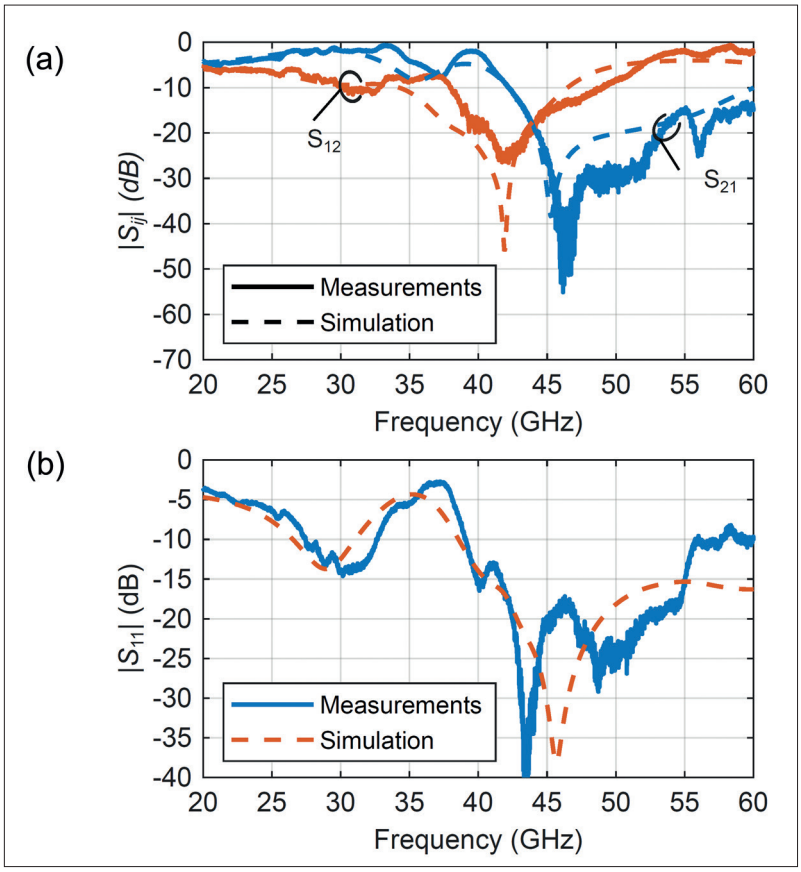

Fig. 5 a–b Measured and simulated S-parameters: forward and backward transmission coefficients S_{21} and S_{12} **(a)**; and reflection coefficient S_{11} **(b)** vs. frequency of LTCC multilayer circulator with drop-in Sr-ferrite

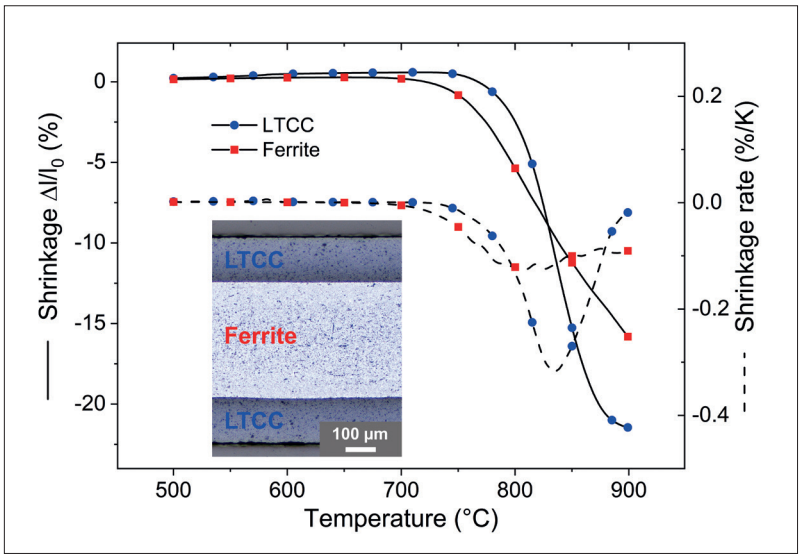

Fig. 6 Shrinkage and shrinkage rate of $BaSc_{0,5}Fe_{11,5}O_{19}$ ferrite and CT708 LTCC tapes; inset: optical microscopy micrograph of a cofired CT708 – ferrite – CT708 multilayer stack

were characterised using XRD (Fig. 7 a). Since the magnetic field during drying is oriented perpendicularly to the film plane, the XRD pattern of the sintered film exhibits high intensity (00l) reflexes indicating strong texturing of the ferrite particles with their c-axis perpendicular to the film plane (Fig. 7 a). Besides the (006) and (008) reflexes, also the (107) appears with high intensity. Pole figure measurements of (006),

(107) and (114) peaks confirm the presence of a significant degree of texture in the films (Fig. 7 b). Examination of the (006) pole figure and the rings observed in (107) and (114) pole figures reveals a strong fibre texture of the film. These results demonstrate that ferrite thick films exhibit strong preferential orientation of the particles with their c-axis perpendicular to the film plane.

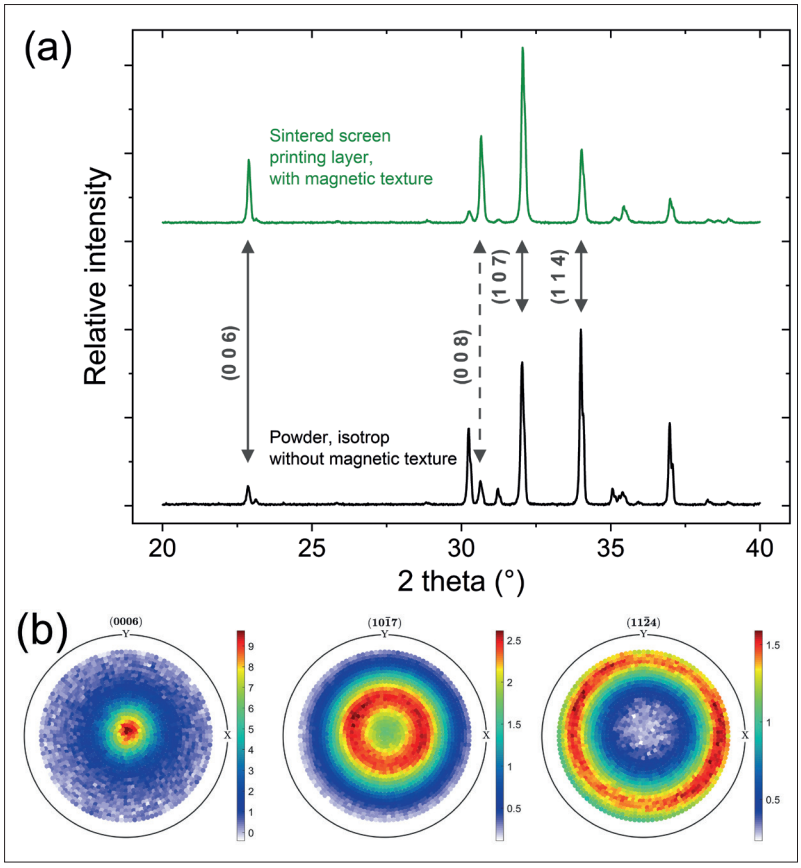

Fig. 7 a–b X-ray diffraction patterns of $BaSc_{0,5}Fe_{11,5}O_{19}$ ferrite isotropic powder (bottom) and textured printed ferrite film (top) **(a)**; XRD pole figures of (006), (107) and (114) reflexes of textured and fired ferrite films **(b)**

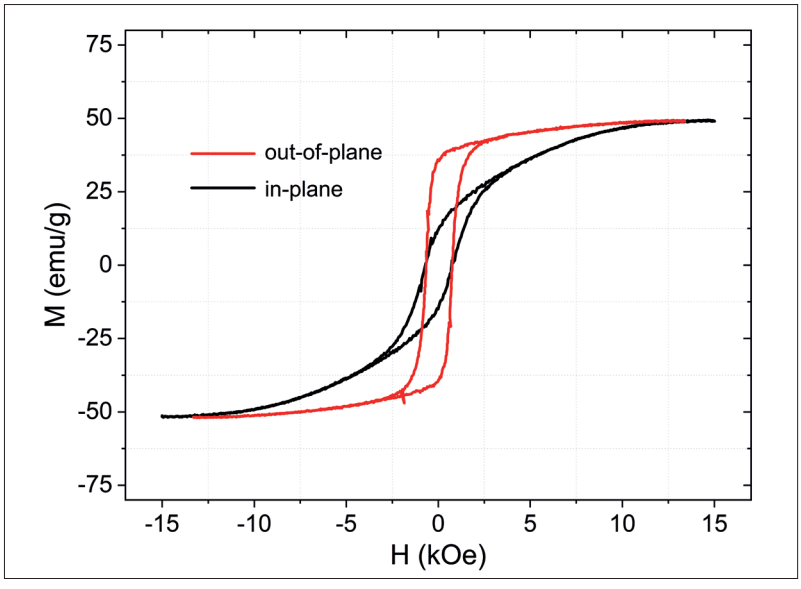

Fig. 8 Room-temperature hysteresis loops (out-of-plane and in-plane) of textured (⊥) Sc-substituted hexagonal ferrite films

The variation of magnetisation of a ferrite film as function of applied field at room temperature, measured with a VSM magnetometer, is shown in Fig. 8. Hysteresis measurements of the textured films (dried with magnetic field perpendicular to film plane) show clear differences between in-plane and out-of-plane (orientation of magnetic field during VSM measurement parallel or perpendicular to film plane, respectively) hysteresis measurements. This is another evidence for significant particle orientation in such printed textured ferrite thick films. To build up multilayer circulators with integrated ferrite films, the Sc-substituted ferrite (x = 0,5) thick films were obtained by multiple printing on CT708 green tape and intermediate drying in a magnetic field. Next, the other layers of CT708 green tape were stacked and laminated. The whole assembly was then cofired at 900 °C with a weight of 1,4 kg on top. Pressure-assisted cofiring is required to avoid warping of the multilayer stacks.

A schematic of the integration of printed ferrite layers in the multilayer circulator is shown in Fig. 9 a, a CT micrograph of circulator structures in Fig. 9 b. The fabricated circulator has a radius of the circular center conductor of r = 990 µm, a width of the microstrip line of w = 125 µm, a substrate thickness of 150 µm and a ferrite film thickness of 60 µm. The material parameters for the deposited ferrite thick film used in simulation were a saturation magnetisation of 150 mT, a line width of 1500 Oe, an internal magnetic field of 8500 Oe, $\varepsilon_r = 5$ and $\tan\delta = 0{,}02$.

The circulator shows an input reflection loss of less than –10 dB and an insertion loss below –10 dB from 30–37 GHz (Fig. 10). The maximum NR effect within this range exceeds 10 dB at 33 GHz.

3-1-3 LTCC integration of ferrite tapes

As a third option, ferrite layers were integrated into the LTCC multilayer stack using ferrite tapes. The integration of a ferrite tape in a LTCC multilayer is schematically illustrated in Fig. 11. The shrinkage behaviour of the ferrite and CT708 LTCC green tapes is shown in Fig. 6. The main shrinkage and the shrinkage rate maxima of both tapes

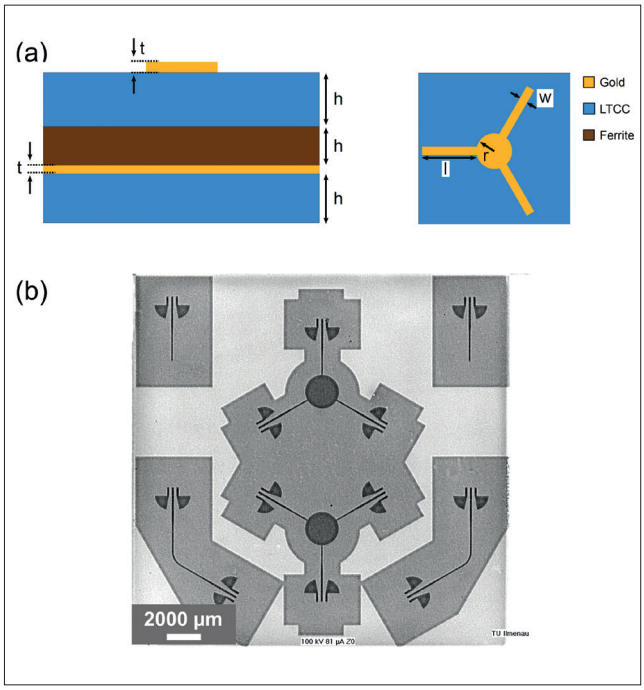

Fig. 9 a–b LTCC circulator integration of printed hexagonal ferrite films: scheme of LTCC circulator with printed ferrite layer **(a)**; and CT top view onto LTCC multilayer circulator with printed ferrite layers **(b)**

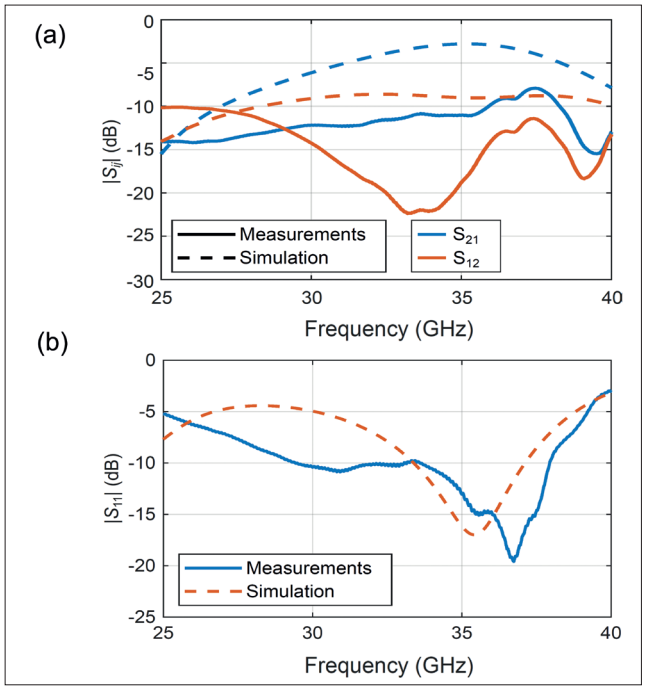

Fig. 10 a–b Measured and simulated S-parameters: forward and backward transmission coefficients S_{21} and S_{12} **(a)**; and reflection coefficient S_{11} **(b)** vs. frequency of LTCC multilayer circulator with printed Sc-substituted hexagonal ferrite layers

appear between 800–900 °C [28]. Cofiring of ferrite and CT708 tapes was performed at 900 °C, and multilayer stacks without cracks or deformations are obtained (Fig. 6, inset).

Measurements of the S-parameters of the fabricated circulator structure showed small non-reciprocity NR only, indicating that significant improvements of the multilayer circulator are needed. One major problem of the present setup is the use of isotropic, non-textured ferrite tapes. To use the full potential of substituted hexagonal microwave ferrites, self-biasing has to be achieved by magnetically texturing the ferrite tapes. Experiments to fabricate oriented ferrite tapes through integration of a magnetic field in the drying channel of the tape casting machine is part of ongoing work.

4 Conclusions

Integration of hexagonal ferrites with ferromagnetic resonance frequencies in the K- and K_a-bands into LTCC multilayer architectures is a promising option to fabricate miniaturised self-biasing circulators for applications in satellite communication. We have investigated different LTCC technology routes for integration of hexagonal microwave ferrites.

Sintered and textured ferrite pellets can be integrated in LTCC multilayer structures as drop-in ferrites and subsequent cofiring. Technological aspects of precise positioning the ferrite pellet and error-free cofiring of the assemblies were demonstrated. Circulators with promising microwave properties were obtained. Integration of printed ferrite films represents another promising option. Textured thick films of Sc-substituted M-type ferrites were prepared by screen-printing, drying in a static magnetic field, and cofiring at 900 °C. The preferred orientation of the films was characterised by XRD texture analysis and VSM measurements. An oriented ferrite film of 60 µm thickness was applied in a LTCC circulator with S-parameters that demonstrate the function of the device. Integration of ferrite tapes in LTCC multilayer structures was achieved through cofiring of ferrite and CT708 tapes with adjusted shrinkage and thermal expansion behaviour.

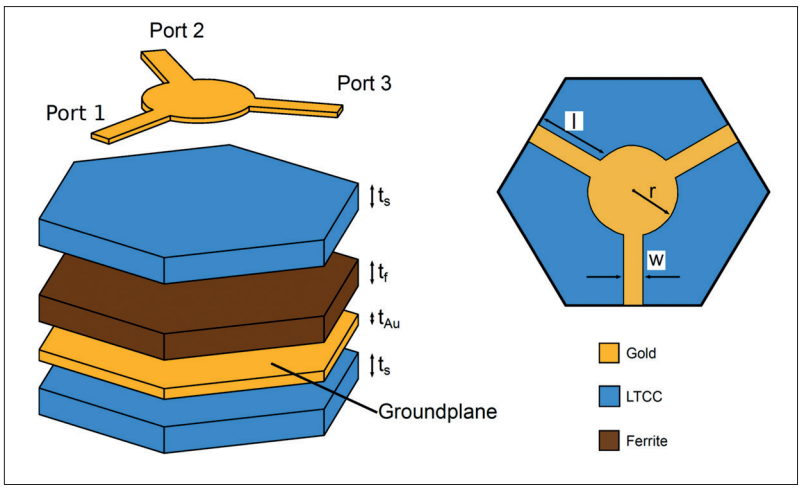

Fig. 11 LTCC multilayer circulator with integration of Sc-substituted hexagonal ferrite tape

The results demonstrate the potential of sintered ferrites and ferrite thick films as self-biased magnetic materials in non-reciprocal circulator devices in the 30 GHz frequency region. Further optimization of ferrite microstructure and microwave properties, film quality and circulator design is required for the fabrication of self-biasing LTCC circulators with competitive performance.

Acknowledgments

The authors acknowledge funding and support of the German Aerospace Center (DLR) on behalf of the German Federal Ministry of Economics and Technology (BMWi) under grants 50YB1308 and 50YB1305.

References

[1] Wolff, I.; et al.: IEEE Microwave Mag. **18** (2018) 36-47

[2] Kulke, R.; et al.: Ceramic microwave circuits for satellite communication. J. Microelectronics Electronic Packaging **6** (2009) [1] 27–31

[3] Klein, T.; Kulke, R.; Wolff, I.: LTCC: A space qualified integration and packing technology for millimeter wave systems. Workshop for the International Microwave Symposium (IMS), Montreal, Canada, 22 June 2012

[4] Smit, J.; Wijn, H.P.J.: Les Ferrites. Bibliothèque Technique Philips, Paris, 1961

[5] Kojima, H.; Fundamental properties of hexagonal ferrites. In: Wohlfahrt, E.P. (ed.), Ferromagnetic Materials, Vol. 3, Amsterdam 1982, 305–391

[6] Pardavi-Horvat, M.: Microwave applications of soft ferrites. J. Magn. Magn. Mater. **215–216** (2000) 171–183

[7] Özgür, Ü.; Alivov, Y.; Morkoc, H.: Microwave ferrites, part 1: fundamental properties. J. Mater. Sci. Mater. Electron. **20** (2009) 789–834

[8] Harris, V.; et al.: Recent advances in processing and applications of microwave ferrites. J. Magn. Magn. Mater. **321** (2009) 2035–2047

[9] Harris, V.: Modern microwave ferrites. IEEE Trans. Magn. **48** (2012) 1075–1104

[10] Silber, L.M.; Tsantes, E.; Angelo, P.: Ferromagnetic resonance in a uniaxial anisotropic ferrite: $BaFe_{12}O_{19}$. J. Appl. Phys. **38** (1967) 5315–5318

[11] Dionne, G.F.; Fitzgerald, J.F.: Magnetic hysteresis properties of BaFe12–xInxO19 ceramic ferrites with c-axis oriented grains. J. Appl. Phys. **70** (1991) 6140–6142

[12] Röschmann, P.; et al.: Anisotropy fields and FMR linewidth in single crystal Al, Ga and Sc substituted hexagonal ferrites with M structure. Mat. Res. Bull. **19** (1984) 385–392

[13] Wang, A.; et al.: Magnetic and atomic structure parameters of Sc-doped barium hexagonal ferrites. J. Appl. Phys. **103** (2008) 07E511

[14] Bierlich, S.; et al.: Low-temperature sintering and magnetic properties of Sc- and In-substituted M-type hexagonal barium ferrites for microwave applications. Mater. Res. Bull. **86** (2017) 19–23

[15] Heidenreich, M.; et al.: Ga-, Y-, and Sc-substituted M-type ferrites for self-biasing circulators in LTCC microwave modules. AIP Advances **10** (2020) 025315

[16] Harris, V.; A. Sokolov, A.: The self-biased circulator: ferrite material design and process considerations. J. Supercond. Nov. Magn. **32** (2019) 97–108

[17] O'Neil, B.; Young, J.L.: Experimental investigation of a self-biased microstrip circulator. IEEE Trans. Microwave Theor. Techn. **57** (2009) 1669–1674

[18] Chen, Y.; et al.: Screen printed thick self-biased, low-loss, barium hexaferrite films by hot-press sintering. J. Appl. Phys. **100** (2006) 043907

[19] Bierlich, S.; et al.: Sintering, microwave properties, and circulator applications of textured Sc-substituted M-type ferrite thick films. J. Europ. Ceram. Soc. **39** (2019) 3077–3081

[20] Bachmann, F.; Hielscher, R.; Schaeben, H.: Texture analysis with MTEX – free and open source software toolbox. Solid State Phenomena **160** (2010) 63–68

[21] Albanese, G.; et al.: Mössbauer investigation of In and Sc substituted barium hexaferrite. Appl. Phys. A **26** (1981) 45–50

[22] Aleshko-Ozhevskii, O.P.; et al.: Helicoidal antiphase spin ordering in hexagonal ferrites of the BaScxFe12–x019 system. Sov. Phys. JETP **28** (1969) 425–430

[23] Ustinov, A.B.; et al.: Al substituted Ba hexaferrite single-crystal films for millimeter wave devices. J. Appl. Phys. **105** (2009) 023908

[24] Lotgering, F.K.: Topotactical reactions with ferrimagnetic oxides having hexagonal crystal structures. J. Inorg. Nucl. Chem. **9** (1959) 113–123

[25] Weiss, J.A.; Watson, N.G.; Dionne, G.F.: New uniaxial ferrite millimeter-wave junction circulators. IEEE MTT-S Digest, **C2** (1989) 145–148

[26] Laur, V.; et al.: Self-biased Y-junction circulators using Lanthanum- and Cobalt-substituted Strontium Hexaferrites. IEEE Trans. MTT **63** (2015) 4376–4381

[27] Gitzel, W.M.; et al.: Experimental study of self-biased Q-/V-band circulators in LTCC-Technology. Private communication

[28] Capraro, B.; Heidenreich, M.; Töpfer, J.: Large thermal expansion LTCC system for cofiring with integrated functional ceramics layers. Mater. **15** (2022) 564

www.cfi.de